

How massless are Weyl fermions in Weyl semimetals?

Amar Bharti,¹ Misha Ivanov,² and Gopal Dixit^{1,2,*}

¹*Department of Physics, Indian Institute of
Technology Bombay, Powai, Mumbai 400076, India*

²*Max-Born Institut, Max-Born Straße 2A, 12489 Berlin, Germany*

(Dated: July 26, 2023)

Abstract

Circularly polarized light fails to generate currents in inversion-symmetric Weyl semimetals with degenerate Weyl nodes. While each node generates current with the direction depending on its chirality, the two currents in the two degenerate nodes of opposite chirality cancel each other. By extension, it is also generally expected that the currents generated at the same Weyl node by the fields of opposite helicity should also observe mirror symmetry and cancel. Surprisingly, here we find that this is not the case. The origin of this effect lies in the nonlinear energy dispersion, which manifests strongly already very close to the Weyl nodes, where linear dispersion is expected to hold and the Weyl fermions are thus expected to be massless. A scheme based on using a trefoil field composed of a counterrotating fundamental and its second harmonic is proposed to control the induced asymmetry at a chiral node from positive to negative, including zero.

* gdixit@phy.iitb.ac.in

Condensed matter systems provide attractive platforms to realize exotic particles, originally proposed in high-energy physics. Weyl semimetals are one such system in which low-energy collective excitations are governed by massless Weyl fermions which appear in pairs of opposite chirality [1]. These fermions exhibit novel phenomena, such as negative magnetoresistance [2–4], the chiral magnetic effect [5–7], the quantized circular photogalvanic effect [8, 9], and the Hall effect [10–13], among others [14–22]. Moreover, Weyl fermions are promising for upcoming quantum technologies at room temperature [23–25].

Light-driven optical response has played a pivotal role in understanding and probing exotic properties of Weyl semimetals [26–32]. One such optical response is circularly polarized light-driven selective excitations in the vicinity of the Weyl nodes. The excitation process depends on the chirality of the Weyl fermions and the helicity of circularly polarized light [33]. Helicity-driven selective excitations in broken inversion-symmetric Weyl semimetals lead to population asymmetry around the Weyl nodes and the circular photogalvanic effect: the generation of current upon irradiation with circular light [27, 34, 35]. Broken inversion symmetry in Weyl semimetals is a prerequisite to ensure noncancellation of the contribution from a pair of chiral Weyl nodes. Thus, when a measurement of coupling between the massless fermions and circularly polarized light is integrated over both nodes, the nonzero result arises only in the inversion-broken Weyl semimetals [27].

Since this conclusion assumes perfectly massless Weyl fermions, i.e., a gapless system with a perfectly linear dispersion near the nodes, it welcomes a question: how quickly is this assumption violated as one moves away from the exact location of the node? Note that deviations from linear dispersion imply that even for gapless nodes, the mass becomes nonzero as soon as one moves away from the degenerate point. Can circularly polarized light with opposite helicity generate non-mirror-symmetric excitations in inversion-symmetric Weyl semimetals once the nonlinearity of the band structure is taken into account, even near the Weyl nodes? We show that the answer to the latter question is positive.

We begin with the perfectly massless Weyl fermions, where the population induced around the chiral Weyl node with $\chi = 1$ by right circularly polarized light is superimposable with that of $\chi = -1$ induced by the left circularly polarized light and vice versa. These populations provide the reference for the more general case of nonlinear band dispersion. Once quadratic corrections to the Weyl equation are included, helicity-sensitive asymmetric excitations becomes nonzero and significant already at the Weyl nodes. That is, the excitation

generated with one helicity at the $\chi = 1$ node is no longer superimposable with that generated by the opposite helicity at the $\chi = -1$ node and the excitations at a given node for light with opposite helicities are not mirror symmetric. The same result obtains for the more general inversion-symmetric Hamiltonian of a Weyl semimetal. While the induced asymmetry reduces when decreasing the light frequency, so that the resonant excitations are located very close to the node, it still remains substantial. Last but not least, we devise a scheme based on two-color counterrotating circularly polarized light to control the helicity-sensitive asymmetric excitation. Our control scheme can tailor the asymmetry from positive to zero to negative.

A Hamiltonian for a type-I Weyl semimetal can be written as [36]

$$\mathcal{H}(\mathbf{k}) = 2t_x \cos(k_x a) \sigma_x + 2t_y \cos(k_y a) \sigma_y + 2t_z [\cos(k_z a) - \alpha - \beta \sin(k_x a) \sin(k_y a)] \sigma_z, \quad (1)$$

where t 's are hopping parameters, σ 's are Pauli matrices, and α and β are dimensionless parameters. The Hamiltonian corresponds to an inversion-symmetric Weyl semimetal with broken time-reversal symmetry [36]. To make our discussion simple, we have considered $t_{x,y,z} = t$ and $\alpha = \beta$. Diagonalization of Eq. (1) yields the band structure shown in Fig. 1(a). The two Weyl nodes are positioned at $W_{1,2} = (\frac{\pi}{2a}, -\frac{\pi}{2a}, \pm\frac{\pi}{2a})$, i.e., $(0.5, 0, \pm 0.25)$ in reduced coordinates [37], and are at the Fermi level. The energy contours in their vicinity in the $k_x - k_y$ plane are isotropic [see Fig. 1(b)], so that light-induced excitation should yield a symmetric population.

Let us first focus on the linear part of the band dispersion. Expanding Eq. (1) up to linear terms near the Weyl nodes, we find

$$\mathcal{H}_1(\mathbf{k}) = d_{1,x}(\mathbf{k}) \sigma_x + d_{1,y}(\mathbf{k}) \sigma_y + d_{1,z}(\mathbf{k}) \sigma_z \quad (2a)$$

$$\mathcal{H}_2(\mathbf{k}) = d_{2,x}(\mathbf{k}) \sigma_x + d_{2,y}(\mathbf{k}) \sigma_y + d_{2,z}(\mathbf{k}) \sigma_z \quad (2b)$$

Here, \mathbf{k} denotes the deviation from the Weyl node [for both nodes, Eqs. (2a) and (2b)], $d_{1(2),x}(\mathbf{k}) = v(-k_x a)$, $d_{1(2),y}(\mathbf{k}) = v(k_y a)$, and $d_{1(2),z}(\mathbf{k}) = v[-(+)\tilde{k}_z a]$, where $-\tilde{k}_z(+\tilde{k}_z)$ is measured relative to the Weyl node 1 (2), and $v = 2t$. The above Hamiltonian in Eq. (2) represents the Weyl equation and can be written as $\mathcal{H}_w = v \mathbf{k} \cdot \boldsymbol{\sigma}$. As pointed above, the two Weyl nodes described by $\mathcal{H}_1(\mathbf{k})$ and $\mathcal{H}_2(\mathbf{k})$ are degenerate and only differ by chirality, which is defined as $\chi = \text{sgn}(d_x \cdot d_y \times d_z)$. The Weyl nodes 1 and 2 have $\chi = 1$ and -1 , respectively.

Light-driven electronic excitation in a Weyl semimetal is simulated using the density matrix approach within the semiconductor Bloch equations framework as discussed in Refs. [32,

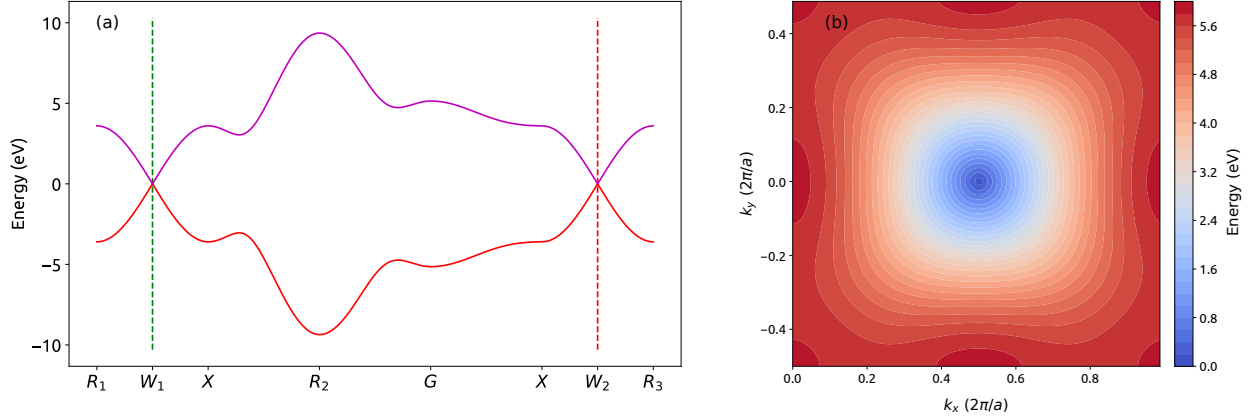


FIG. 1. (a) Energy dispersion along high-symmetry points of an inversion-symmetric Weyl semimetal as given in Eq. (1). (b) Energy contour around one of the Weyl nodes in $k_x - k_y$ plane (Weyl planes). The hopping parameter is $t = 1.8$ eV and the lattice parameters are $a = 6.28$ Å and $\beta = 0.8$. The lattice vectors are $a_1 = (a, -a, 0)$, $a_2 = (a, a, 0)$, $a_3 = (0, 0, a)$, and the reciprocal vectors are $b_1 = (\pi/a, -\pi/a, 0)$, $b_2 = (\pi/a, \pi/a, 0)$, $b_3 = (0, 0, 2\pi/a)$, leading to reduced coordinates for the high-symmetry points as follows: $R_1(\pi/2a, -\pi/2a, -\pi/a)$, $X(\pi/2a, -\pi/2a, 0)$, $R_2(0, \pi/a, -\pi/a)$, $G(0, 0, 0)$, and $R_3(\pi/2a, -\pi/2a, \pi/a)$.

38, 39]. To account for the decoherence between electron and hole during the excitation process, a phenomenological dephasing term with 1.5 fs is introduced. Our findings are robust against the dephasing term ranging from 1.5 to 10 fs.

The conduction band population is obtained by integrating the density matrix in the conduction band after the end of the laser pulse; the population is integrated over k_x and k_y , and is shown along the \tilde{k}_z direction, where $\tilde{k}_z = 0$ is the Weyl plane which contains both chiral Weyl nodes, for Eq. (2). We used ~ 100 fs long circularly polarized pulses with intensity 10^{11} W/cm² and wavelength 3.2 μm (i.e., $\omega = 0.39$ eV); different wavelengths upto 10.6 μm (i.e., $\omega = 0.12$ eV) were also studied, with the results described below.

Figure 2 shows the final population around the two Weyl nodes in the conduction band after the end of the pulse, for $\chi = -1$ (a) and $\chi = 1$ (b) calculated for the Hamiltonians in Eqs. (2a) and (2b), respectively. As expected, the population asymmetry is zero at $\tilde{k}_z = 0$ and is mirror symmetric with respect to changing either the light helicity or the chirality of the node. In particular, the population at $\chi = -1$ induced by the left circularly polarized (LCP) pulse is the same as that induced at $\chi = +1$ by the right circularly polarized (RCP)

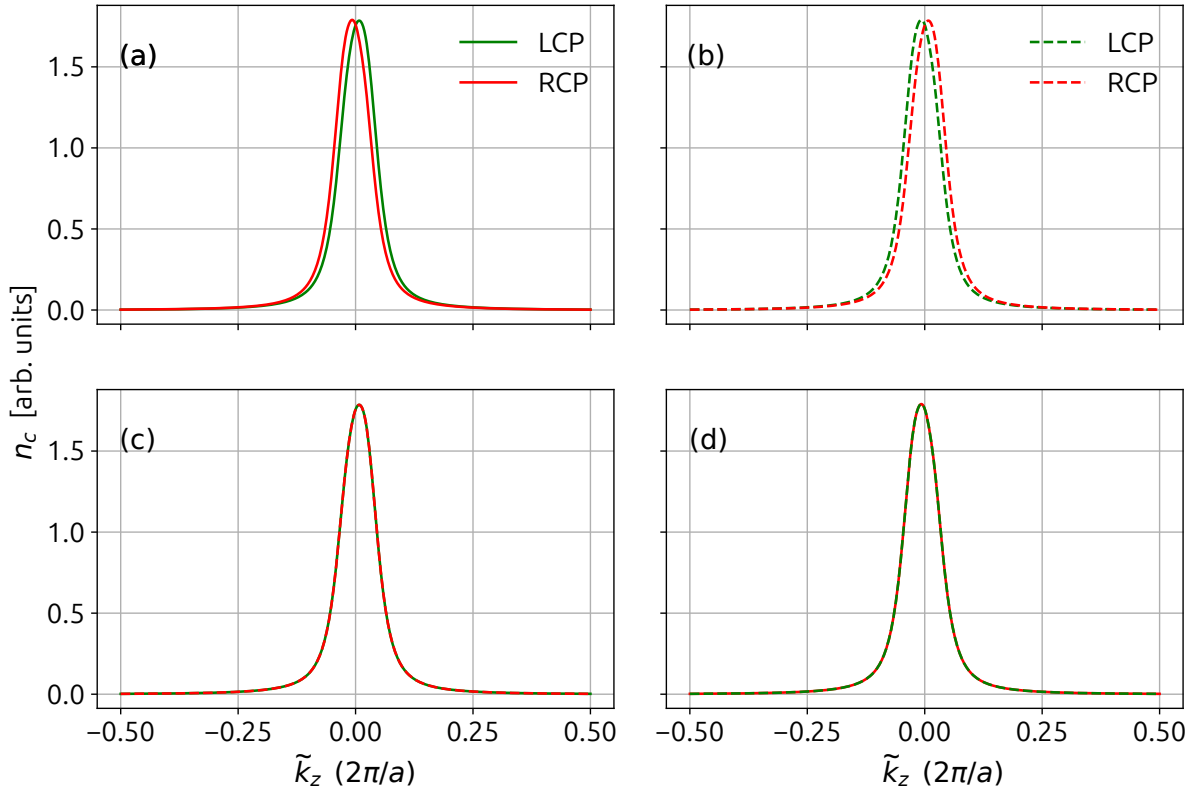


FIG. 2. Residual population in the conduction band (n_c) after the end of the left-handed circularly polarized (LCP) and right-handed circularly polarized (RCP) light around a Weyl node with (a) $\chi = -1$ and (b) $\chi = 1$. (c) Comparison of the residual populations from a Weyl node with $\chi = -1$ due to LCP, and from a Weyl node with $\chi = 1$ due to RCP. (d) Same as (c) for a Weyl node with $\chi = -1$ due to RCP, and from a Weyl node with $\chi = 1$ due to LCP. The Weyl nodes with $\chi = -1$ and $\chi = 1$ are described by Eq. (2).

pulse; see Fig. 2(c). The same is true for the population induced by the RCP at $\chi = -1$ compared to the population induced by LCP near $\chi = 1$; see Fig. 2(d).

Having established this reference, we now go beyond the linear approximation and expand Eq. (1) to the second order, resulting in the following expression,

$$\tilde{\mathcal{H}}_1(\mathbf{k}) = d_{1,x}\sigma_x + d_{1,y}\sigma_y + \tilde{d}_{1,z}\sigma_z, \quad (3a)$$

$$\tilde{\mathcal{H}}_2(\mathbf{k}) = d_{2,x}\sigma_x + d_{2,y}\sigma_y + \tilde{d}_{2,z}\sigma_z, \quad (3b)$$

where $\tilde{d}_{1(2),z}(\mathbf{k}) = v \left[-(+) \tilde{k}_z a \right] - \tilde{v} \left[\frac{(k_x a)^2 + (k_y a)^2}{2} \right]$ with $\tilde{v} = 2t\alpha$. The \tilde{d}_z component now contains additional terms quadratic in k_x and k_y , whereas d_x and d_y remain identical in

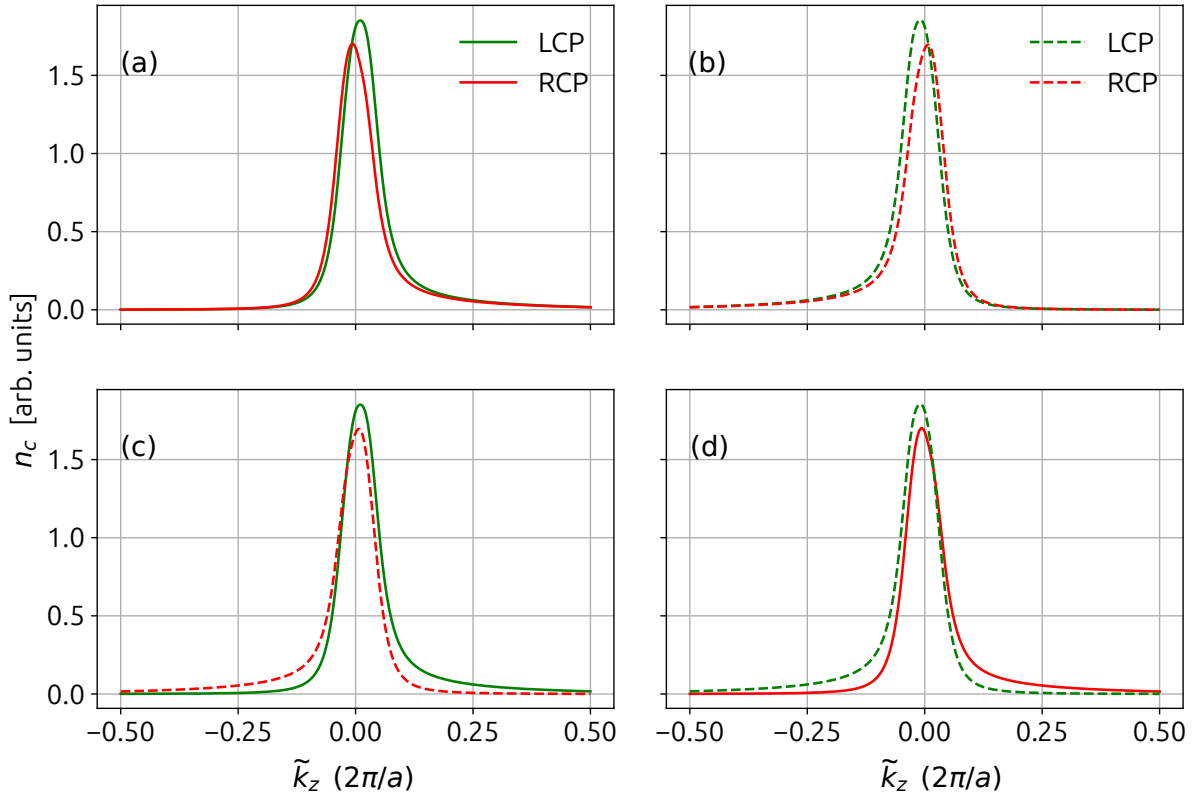


FIG. 3. Same as in Fig. 2 for the Weyl nodes with $\chi = -1$ and $\chi = 1$, but now using the Hamiltonian Eq. (3) which includes the quadratic terms.

both the equations.

The quadratic terms affect the final population already in the immediate vicinity of the Weyl nodes as visible from Figs. 3(a) and 3(b). The mirror symmetry upon changing the handedness of the Weyl node is, of course, preserved: the population near $\chi = -1$ is mirror symmetric with that near $\chi = +1$ with respect to changing $\tilde{k}_z \rightarrow -\tilde{k}_z$. However, for a given Weyl node, the peaks of the populations induced by RCP and LCP light do not coincide. Similarly, the excitation induced near the $\chi = -1$ node by LCP pulse does not overlap with the excitation induced near the $\chi = +1$ node by RCP pulse; see Fig. 3(c). Likewise, the excitation induced near the $\chi = +1$ node by the LCP pulse does not overlap with the excitation induced near the $\chi = -1$ node by RCP pulse; see Fig. 3(d). This stands in stark contrast with Fig. 2. The fact that this asymmetry, associated with the deviations from the linear dispersion, arises in the immediate vicinity of the nodes, i.e., in what is supposed to be

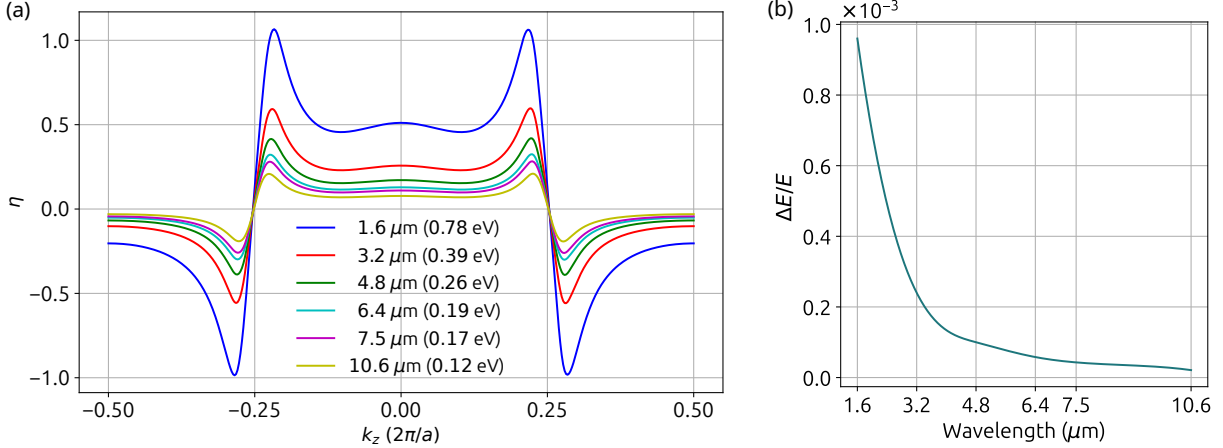


FIG. 4. (a) Normalized population asymmetry (η) as a function of the wavelength of the circularly polarized driving pulse with intensity 5×10^9 W/cm². (b) Nonlinear correction (ΔE) to the energy (E) obtained from the linear dispersion. The simulations use the full Hamiltonian given in Eq. (1).

the zero-mass region, raises the question posed in the title of this Letter: How massless are the Weyl fermions under practical conditions of typical laser wavelengths and intensities?

Since the deviations from the massless behavior could have come from our specific choice of the laser wavelength and intensity, which could have forced the electrons to explore the nonlinear parts of the dispersion, we will scan the laser intensity and wavelength while using the full Hamiltonian given in Eq. (1). Below we shall use normalized population asymmetry defined as

$$\eta = \frac{n_c^\circ - n_c^\circ}{(n_c^\circ + n_c^\circ)/2}, \quad (4)$$

where n_c° (n_c°) is the final population due to LCP (RCP) light along k_z , integrated in the $k_x - k_y$ plane.

Figure 4(a) shows η for the driving wavelengths λ from 1.6 μm to 10.6 μm , which allows one to access different parts of energy dispersion during the excitation. We see that for all λ the asymmetry η is nonzero around the Weyl nodes at $k_z = \pm 0.25$. While the asymmetry reduces with λ , even for the longest wavelength substantial values of η at the levels $\sim 10\%$ arise in the immediate vicinity of the Weyl nodes. We note that the deviation from linear dispersion for the wavelength studied is below 0.001 shown in Fig. 4(b), while the circular dichroism asymmetry induced is several orders of magnitude higher as in Fig. 4(a).

Figure 5(a) shows the dependence of η on laser intensity, for $\lambda = 3.2$ μm . Notably, we find

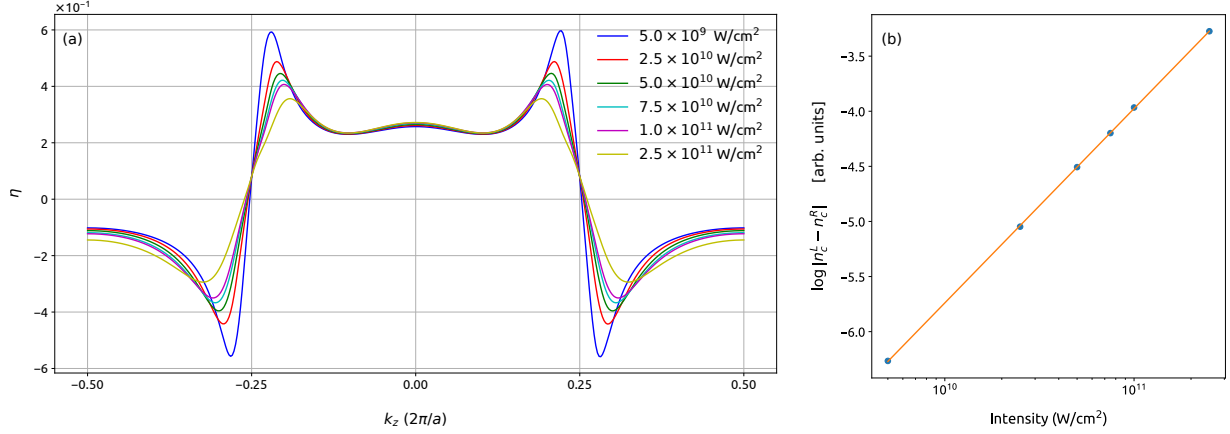


FIG. 5. (a) Variations of the normalized population asymmetry (η) for different intensities of the circularly polarized light. (b) Logarithm of the difference in the population around a given Weyl node excited by the left- or right-handed circularly polarized light, as a function of the laser’s intensity. The slope of the fitted line is 0.8, i.e., is below unity expected for linear processes. The driving light wavelength is $3.2 \mu\text{m}$. The simulations use the full Hamiltonian given in Eq. (1).

that the asymmetry is nonzero exactly at the Weyl node, where the dispersion is linear. This is true for all laser intensities, with the position of the zero asymmetry moving away from the node with increasing intensity. The another surprise is that the asymmetry decreases with increasing intensity, i.e., when the electron is driven to explore a wider range of the Brillouin zone, where the dispersion nonlinearity is stronger. This observation is supported by Fig. 5(b), which shows that the intensity dependence of the non-normalized asymmetry is sublinear, with the slope 0.8.

At this point, it is natural to explore the possibilities to control the ratio of the asymmetry induced by LCP and RCP light at a given node. To this end, we apply $\omega - 2\omega$ counterrotating circularly polarized laser pulses with the total vector potential given by

$$\mathbf{A}(t) = \frac{A_0 f(t)}{\sqrt{2}} ([\cos(\omega t + \phi) + \mathcal{R} \cos(2\omega t)] \hat{\mathbf{e}}_x + [\sin(\omega t + \phi) - \mathcal{R} \sin(2\omega t)] \hat{\mathbf{e}}_y). \quad (5)$$

The ratio between the two electric fields is controlled by \mathcal{R} , and ϕ describes the subcycle relative phase between the ω and 2ω pulses. In recent years, $\omega - 2\omega$ circularly polarised pulses have been employed to control the valley asymmetry in pristine graphene [40, 41].

The population excited by $\omega - 2\omega$ counterrotating pulses is shown in Fig. 6, with the fundamental wavelength $\lambda = 3.2 \mu\text{m}$. For $\mathcal{R} = 0.2$, the RCP-LCP combination generates

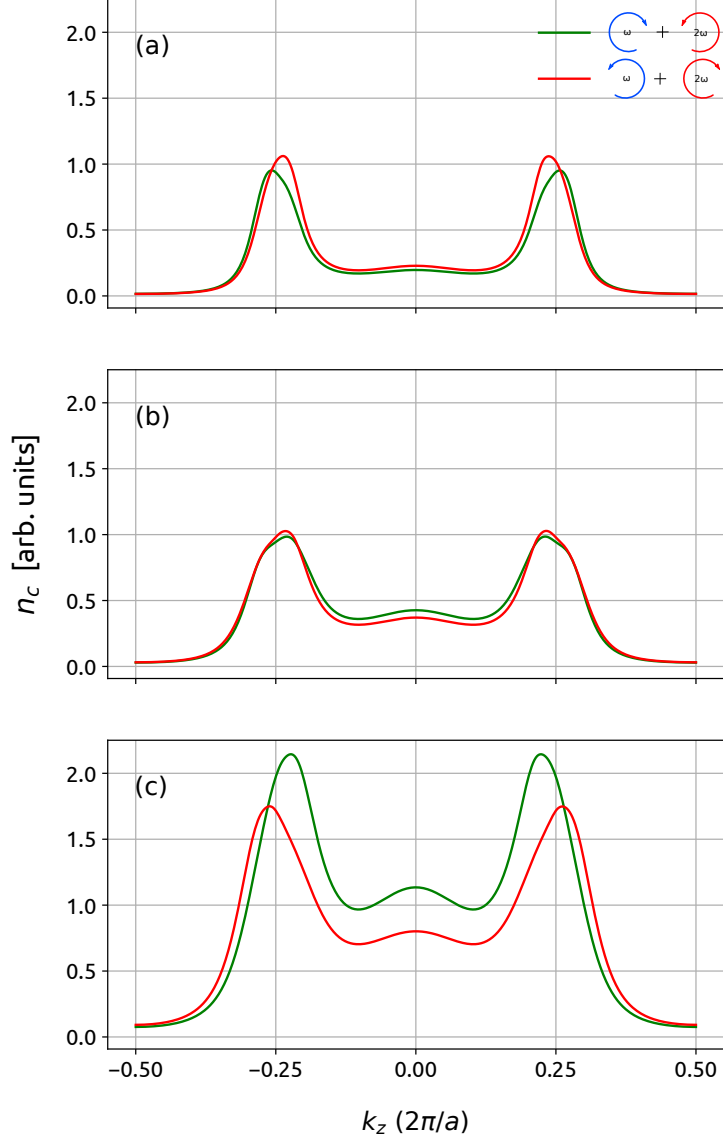


FIG. 6. Residual conduction-band population for different ratio (\mathcal{R}) of the two-color $\omega - 2\omega$ laser pulses: (a) $\mathcal{R} = 0.2$, (b) $\mathcal{R} = 0.5$, and (c) $\mathcal{R} = 1.0$. Intensity and wavelength of the ω pulse are 5×10^{10} W/cm² and 3.2 μm , respectively.

more excitation than the LCP-RCP combination; see Fig. 6(a). Moreover, the peak induced by RCP-LCP combination leans toward the center of the Brillouin zone. As \mathcal{R} changes from 0.2 to 0.5, both combinations yield almost similar population. However, the peaks due to LCP-RCP combination change its direction and peaked toward the center. The situation reverses for $\mathcal{R} = 1$ where the LCP-RCP combination generates higher excitation than the RCP-LCP combination; see Fig. 6(c). The reason behind such behavior is the interplay of

the two competing resonant processes driven by LCP and RCP light, which is controlled by changing \mathcal{R} . Thus, the ratio and the behavior of the residual population can be controlled by tailoring the value of \mathcal{R} in $\omega - 2\omega$ counterrotating pulses.

In conclusion, we have demonstrated the generation of helicity-sensitive population in an inversion-symmetric Weyl semimetal, which is not symmetric with respect to the helicity of the driving circular light. The effect is general and persists for different wavelengths and intensities. Even for the longest wavelegnth and weakest intensities studied, it is triggered by the deviations of the Weyl fermion mass from zero, even in the immediate vicinity of the Weyl node. The origin of this phenomenon is embedded in the Berry connection, which remains unaffected by any modifications in the Hamiltonian of the Weyl semimetal [42]. We have proposed a way to control and manipulate the asymmetric population using counterrotating bicircular light, which allow tailoring the asymmetry from positive to negative via nearly zero. The asymmetric residual population can be probed via time- and angle-resolved photoemission spectroscopy in a pump-probe setup [43].

G. D. acknowledges financial support from SERB India (Project No. MTR/2021/000138).

-
- [1] N. Armitage, E. Mele, and A. Vishwanath, *Reviews of Modern Physics* **90**, 015001 (2018).
 - [2] S. Parameswaran, T. Grover, D. Abanin, D. Pesin, and A. Vishwanath, *Physical Review X* **4**, 031035 (2014).
 - [3] X. Huang, L. Zhao, Y. Long, P. Wang, D. Chen, Z. Yang, H. Liang, M. Xue, H. Weng, Z. Fang, *et al.*, *Physical Review X* **5**, 031023 (2015).
 - [4] C.-L. Zhang, S.-Y. Xu, I. Belopolski, Z. Yuan, Z. Lin, B. Tong, G. Bian, N. Alidoust, C.-C. Lee, S.-M. Huang, *et al.*, *Nature Communications* **7**, 10735 (2016).
 - [5] M. Vazifeh and M. Franz, *Physical Review Letters* **111**, 027201 (2013).
 - [6] Q. Li, D. E. Kharzeev, C. Zhang, Y. Huang, I. Pletikosić, A. Fedorov, R. Zhong, J. Schneeloch, G. Gu, and T. Valla, *Nature Physics* **12**, 550 (2016).
 - [7] S. Kaushik, D. E. Kharzeev, and E. J. Philip, *Physical Review B* **99**, 075150 (2019).
 - [8] F. De Juan, A. G. Grushin, T. Morimoto, and J. E. Moore, *Nature Communications* **8**, 15995 (2017).
 - [9] D. Rees, K. Manna, B. Lu, T. Morimoto, H. Borrmann, C. Felser, J. Moore, D. H. Torchinsky,

- and J. Orenstein, *Science advances* **6**, eaba0509 (2020).
- [10] A. Burkov, *Physical Review Letters* **113**, 187202 (2014).
- [11] C.-K. Chan, P. A. Lee, K. S. Burch, J. H. Han, and Y. Ran, *Physical Review Letters* **116**, 026805 (2016).
- [12] C. Shekhar, N. Kumar, V. Grinenko, S. Singh, R. Sarkar, H. Luetkens, S.-C. Wu, Y. Zhang, A. C. Komarek, E. Kampert, et al., *Proceedings of the National Academy of Sciences* **115**, 9140 (2018).
- [13] H. Li, H. Liu, H. Jiang, and X. Xie, *Physical Review Letters* **125**, 036602 (2020).
- [14] Y. Gao, S. Kaushik, E. Philip, Z. Li, Y. Qin, Y. Liu, W. Zhang, Y. Su, X. Chen, H. Weng, et al., *Nature Communications* **11**, 720 (2020).
- [15] G. B. Osterhoudt, L. K. Diebel, M. J. Gray, X. Yang, J. Stanco, X. Huang, B. Shen, N. Ni, P. J. Moll, Y. Ran, et al., *Nature Materials* **18**, 471 (2019).
- [16] Y. Okamura, S. Minami, Y. Kato, Y. Fujishiro, Y. Kaneko, J. Ikeda, J. Muramoto, R. Kaneko, K. Ueda, V. Kocsis, et al., *Nature Communications* **11**, 4619 (2020).
- [17] J. Liu, F. Xia, D. Xiao, F. J. Garcia de Abajo, and D. Sun, *Nature Materials* **19**, 830 (2020).
- [18] Y.-Y. Lv, X. Li, B.-B. Zhang, W. Deng, S.-H. Yao, Y. Chen, J. Zhou, S.-T. Zhang, M.-H. Lu, L. Zhang, et al., *Physical Review Letters* **118**, 096603 (2017).
- [19] D. Hamara, G. F. Lange, F. N. Kholid, A. Markou, C. Felser, R.-J. Slager, and C. Ciccarelli, *arXiv preprint arXiv:2302.07286* (2023).
- [20] A. Bharti and G. Dixit, *Physical Review B* **107**, 224308 (2023).
- [21] U. Khanna, A. Kundu, S. Pradhan, and S. Rao, *Physical Review B* **90**, 195430 (2014).
- [22] O. Neufeld, H. Hübener, G. Jotzu, U. De Giovannini, and A. Rubio, *arXiv preprint arXiv:2304.05186* (2023).
- [23] D. E. Kharzeev and Q. Li, *arXiv:1903.07133*.
- [24] D. Kharzeev and Q. Li, “Quantum computing using chiral qubits,” (2020), uS Patent 10,657,456.
- [25] J. Chen, Y. Zhou, J. Yan, J. Liu, L. Xu, J. Wang, T. Wan, Y. He, W. Zhang, and Y. Chai, *Nature Communications* **13**, 7758 (2022).
- [26] N. Sirica, R. Tobey, L. Zhao, G. Chen, B. Xu, R. Yang, B. Shen, D. Yarotski, P. Bowlan, S. Trugman, et al., *Physical Review Letters* **122**, 197401 (2019).
- [27] Q. Ma, S.-Y. Xu, C.-K. Chan, C.-L. Zhang, G. Chang, Y. Lin, W. Xie, T. Palacios, H. Lin,

- S. Jia, *et al.*, *Nature Physics* **13**, 842 (2017).
- [28] J. Ma, Q. Gu, Y. Liu, J. Lai, P. Yu, X. Zhuo, Z. Liu, J.-H. Chen, J. Feng, and D. Sun, *Nature Materials* **18**, 476 (2019).
- [29] B. Lv, T. Qian, and H. Ding, *Reviews of Modern Physics* **93**, 025002 (2021).
- [30] Y.-Y. Lv, J. Xu, S. Han, C. Zhang, Y. Han, J. Zhou, S.-H. Yao, X.-P. Liu, M.-H. Lu, H. Weng, *et al.*, *Nature Communications* **12**, 1 (2021).
- [31] J. Orenstein, J. Moore, T. Morimoto, D. Torchinsky, J. Harter, and D. Hsieh, *Annual Review of Condensed Matter Physics* **12**, 247 (2021).
- [32] A. Bharti, M. Mrudul, and G. Dixit, *Physical Review B* **105**, 155140 (2022).
- [33] R. Yu, H. Weng, Z. Fang, H. Ding, and X. Dai, *Physical Review B* **93**, 205133 (2016).
- [34] E. König, H.-Y. Xie, D. Pesin, and A. Levchenko, *Physical Review B* **96**, 075123 (2017).
- [35] C.-K. Chan, N. H. Lindner, G. Refael, and P. A. Lee, *Physical Review B* **95**, 041104 (2017).
- [36] J.-M. Hou and W. Chen, *Scientific Reports* **6**, 33512 (2016).
- [37] The band structure and the position of the Weyl points obtained from Eq. (1) are periodic with a translation of reciprocal lattice vectors.
- [38] M. Mrudul and G. Dixit, *Physical Review B* **103**, 094308 (2021).
- [39] N. Rana, M. Mrudul, D. Kartashov, M. Ivanov, and G. Dixit, *Physical Review B* **106**, 064303 (2022).
- [40] M. Mrudul, Á. Jiménez-Galán, M. Ivanov, and G. Dixit, *Optica* **8**, 422 (2021).
- [41] M. Mrudul and G. Dixit, *Journal of Physics B* **54**, 224001 (2021).
- [42] B. Sadhukhan and T. Nag, *Physical Review B* **103**, 144308 (2021).
- [43] C. P. Weber, *Journal of Applied Physics* **129**, 070901 (2021).